Canadian Science Publishing
NRC Research Press journals | Publishing Services

Canadian Journal of Chemistry
Revue canadienne de chimie

The application of XANES for the examination of silver, gold, mercury, and sulfur on the daguerreotype surface

Journal:	*Canadian Journal of Chemistry*
Manuscript ID	cjc-2017-0062.R1
Manuscript Type:	Article
Date Submitted by the Author:	04-May-2017
Complete List of Authors:	Kozachuk, Madalena; The University of Western Ontario, Chemistry Martin, Ron; Department of Chemistry Sham, Tsun-Kong; Department of Chemistry, Robinson, Mike; Century Darkroom Nelson, Andrew; University of Western Ontario
Is the invited manuscript for consideration in a Special Issue?:	TK Sham
Keyword:	Daguerreotypes, X-ray absorption spectroscopy, Surface metrology, Surface topology

The application of XANES for the examination of silver, gold, mercury, and sulfur on the daguerreotype surface

M.S. Kozachuk[1*]; R.R. Martin[1]; T.K. Sham[1*]; M. Robinson[2]; A.J. Nelson[3]

1. *Western University, The Department of Chemistry, 1151 Richmond Street, London, Ontario, N6A 5B7, Canada*
2. *Century Darkroom, 245 Carlaw Avenue, Studio 502, Toronto, Ontario, M4M 2S1, Canada*
3. *Western University, The Department of Anthropology, 1151 Richmond Street, London, Ontario, N6A 5B7, Canada*

*Corresponding Author: tel: 1-(519) 661-2111 ext. 86341; fax: 1-519-661-3022; email: mkozachu@uwo.ca (M.S. Kozachuk); tsham@uwo.ca (T.K. Sham)

Abstract X-ray absorption near edge structure (XANES) spectroscopy was used to study a freshly prepared reference daguerreotype surface as the first step in devising improved methods for the conservation of these important historic artifacts. The results are consistent with the formation of alloy image particles. Inter-diffusion of gold and silver has led to the development of a silver-gold alloy; the composition varies with depth. The amount of gold appeared to be elevated in the highlighted regions of the image while shadow regions have lower levels of gold on the surface. The apparent increase in gold within the highlight region may be due to the larger surface area presented by an array of small image particles. The mercury used to develop the daguerreian image showed no evidence of oxidation while a mercury-silver alloy was detected. Sulfur based contaminants are also detected. The implications of these findings are discussed.

KEYWORDS: Daguerreotypes, X-ray absorption spectroscopy, Surface metrology, Surface topology

Graphic Abstract

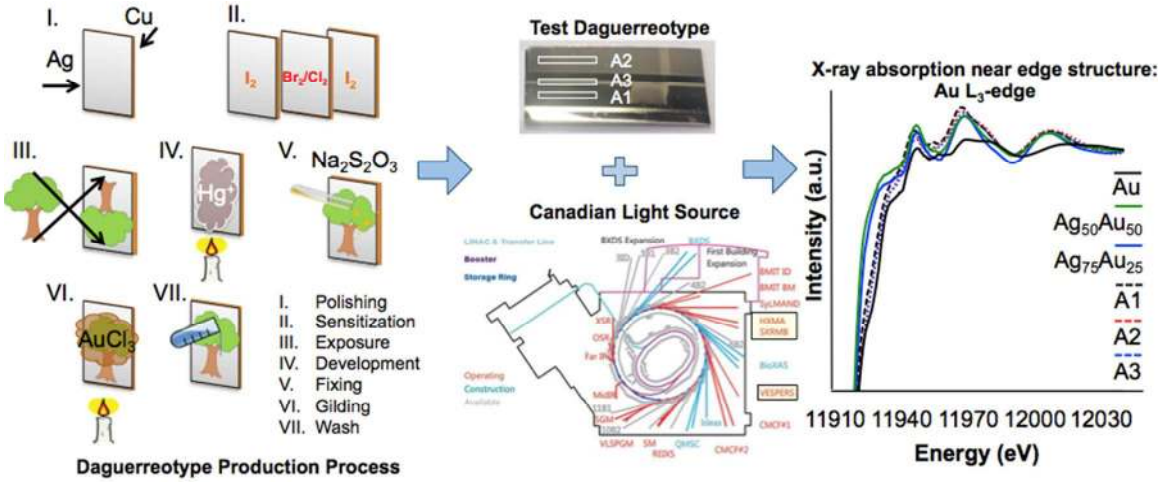

1 Introduction

Invented in 1839 by Louie-Jacques-Mandé Daguerre, the daguerreotype process was used throughout Europe and North America for a span of approximately 25 years. The process consists of rendering a silver surface photosensitive by reaction with iodine vapour. After light exposure the image is developed with mercury vapour. Later refinements included gilding to enhance image contrast [1, 2]. The appearance of the daguerreotype image is the result of the interaction (reflection and scattering) of light with image particles on the surface, formed when the photosensitive plate is exposed to light. Regions that were subjected to bright exposure (i.e., highlight regions) produced image particles of relatively uniform structure and density. Portions of the plate that received little to no exposure (i.e. shadow and dark regions) exhibited image particles with variable size, shape and surface density [3a]. This variation in particle density and shape produce the great range of gray tones that typify daguerreotypes.

Daguerreotypes are prone to tarnish, fogging, white and blue-tinted haze, and black spots termed “daguerreian measles” [3b] that form as a result of reactions leading to the formation of silver compounds including oxides, chlorides, and sulfides, respectively [4]. Sulfur and chlorine are the two elements generally associated with daguerreotype image deterioration in the forms of silver sulfide [5] and silver chloride [6]. The composition of such tarnish has been analyzed using techniques such as diffuse reflectance spectroscopy [7], confocal microscopy [4,8], laser induced breakdown spectroscopy [9], laser ablation mass spectrometry [10], X-ray fluorescence spectroscopy (XRF) [1], two dimensional scanning electron microscopy (SEM) and three-dimensional focused ion beam scanning electron microscopy (FIB-SEM) [2]. These techniques have furthered the understanding of the photo-physico-chemical reactions involved in the formation of the daguerreotype

image as well as the nature of the tarnish formed on these surfaces. This information is important for the conservation, preservation, storage, and display of these artifacts.

The research undertaken here used synchrotron radiation analysis, particularly its X-ray absorption near edge structure (XANES) spectroscopy capabilities, to characterize the chemical environment of the elements on the daguerreotype surface. XANES measures the modulation of the absorption coefficient above an absorption edge when the absorbing atom is placed in a chemical environment; the photoelectron, which is produced by the X-rays, will sample the surrounding atoms in the vicinity of the absorbing atom, bring the information back via back scattering as the X-ray energy increases above the absorption threshold. The result is a XANES spectrum that shows the edge jump (threshold) and resonances resulting from transitions to electronic states that are bound, quasi bound (multiple scattering) and in the continuum (EXAFS), which is set up by the molecular potential of the surrounding atoms. This absorption technique, which is elementally and chemically sensitive, at the resolution provided by the synchrotron source, will provide new information regarding the chemical speciation of the elements of interest on the daguerreian plate. This is the first step in devising a strategy for the conservation of these artifacts. Owing to the chemical composition of the daguerreotype plate, the elements of interest for this study are silver, gold, mercury, and sulfur.

2 Materials and methods

The daguerreotype plate (5 × 1 cm) used in this research (Figure 1) was prepared at Century Darkroom, Toronto (Daguerreotypist, Mike Robinson) using the process described by Humphrey [11]. Once the silver coated copper plate was polished to a mirror finish, the plate was historically exposed to iodine vapour. Bromine and chlorine were later added to the photosensitizing process, which reduced the exposure time from a

few minutes to a few seconds. Once the plate was exposed to the image of interest, the daguerreotype was developed with mercury vapour heated to 70 °C. A sodium thiosulfate wash removed any residual silver halide. The final step involved pouring a gold-chloride-sodium thiosulfate solution over the plate, which was heated from below, depositing gold on the image surface [1, 2, 11]. The range of tones on these test plate is representative of the tones observed on historical daguerreian artifacts. All reported XANES spectra were taken at the labeled locations on the daguerreian test plate (A1: dark region; A2: mid-tone region; A3: bright region).

Three separate beamlines at the Canadian Light Source (CLS) were used to collect the absorption data: SXRMB, VESPERS, and HXMA (Table 1). The beamlines were selected as their respective energy ranges corresponded to the absorption edges of the elements of interest (silver, gold, mercury, and sulfur). On the daguerreotype test plate, SXRMB was utilized to collect the silver (Ag) L_3-edge XANES. The beam was monochromatized by a Si(111) double crystal monochromator and XANES were recorded in the fluorescence yield (FLY) mode using a 13-element Ge detector situated at 45° with respect to the sample stage. Spectra were collected from 3,331 eV to 3,411 eV using a 2.00 eV step size before, a 0.20 eV step size at, and a 0.75 eV step size after the L_3 absorption edge region. Larger step sizes before the edge are chosen so that appropriate background correction can be conducted; a smaller step size is used at the edge to optimize the quality of the data. Step size is chosen based on monochromator and slit resolution. The SXRMB line was also used to collect the sulfur (S) K-edge over an energy range of 2,454 eV to 2,534 eV with a 2.00 eV step size before, a 0.20 eV step size at, and a 0.75 eV step size after the absorption edge. The size of the beam on the sample was 1 mm (vertical) x 4 mm (horizontal) in both measurements.

The gold (Au) and mercury (Hg) L_3-edges were initially examined on the VESPERS beamline using XRF with a microbeam using KB mirrors. The Au L_3-edge XANES spectra were collected from 11,759 eV to 12,150 eV with a step size of 10.00 eV before, a 0.50 eV step size at, and a 0.05 eV step size after the absorption region. The Hg L_3-edge was collected over an energy range of 12,124 eV to 12,400 eV with a step size of 10.00 eV before, a 0.50 eV step size at, and a 0.05 eV step size after the absorption region. For the Hg standard, an aqueous suspension of elemental Hg collected in FLY was utilized. The preparation for this standard is outlined in detail elsewhere [12].

A series of Ag-Au alloys (Table 2), whose preparation is outlined in Bzowski et al. [13], were also analyzed at the CLS using XANES as standards for comparison with the daguerreotype test plate. The Ag L_3-edge was collected at the SXRMB line under the same conditions described above. The Au L_3-edge was analyzed at the HXMA beamline that focuses the beam with a liquid nitrogen cooled double crystal Si(111) monochromator (Kohzu CMJ-1). Further collimation is achieved by using a 1.15 m long water-cooled silicon toroidal focusing mirror. The resulting beam size was 1 mm (vertical) x 10 mm (horizontal).

The Athena software package [14] was used to calibrate, background subtract, normalize, and average all spectra. The true inflection point at the edge was determined by taking the first derivative of each spectrum as well as setting the tangent slope to zero in the second derivative spectrum following the procedure outlined by Ravel [15]. These first derivative inflections were 3,351 eV, 11,919 eV, 12,284 eV, and 2,472 eV for the Ag L_3-edge, Au L_3-edge, Hg L_3-edge, and S K-edge, respectively. A first-order polynomial was fit to the pre- and post-edges of the spectra along with normalizing the edge-jump of

each spectrum to one. A linear combination fit analysis was also performed when appropriate.

3 Results and discussion

3.1 Silver

The Ag L_3-edge XANES (edge jump located at 3,351 eV) is shown in Figure 2. The oscillation magnitude relative to a smooth background is compared to the alloy standards; in general, the magnitude is sensitive to the scattering characteristics of nearest neighbouring atoms. There is no sharp peak at the rising edge, also known as the whiteline (WL), indicating that the Ag d band is full. Metals with partially filled d bands always exhibit an intense resonance historically called whiteline. The oscillations in the spectra at increasing energy above the threshold (labeled II to V) are due to the multiple and single scattering of the photoelectrons by the neighboring Ag atoms. The oscillation patterns within the L_3-edge XANES of the alloy standard and the A1-3 specimen are indicative of a face centered cubic (fcc) structure [13].

Region I is the WL region assigned to the excitation of a $2p_{3/2}$ electron to unoccupied bands just above the Fermi level, which possess both s and d character. The absorption is weak because the 5d bands are full in Ag metal, although the presence of some d character is possible due to s-d hybridization. Regions II – IV can be viewed as multiple scattering resonances given rise by the fcc environment of the Ag atom [13]. The intensity of peak II increases from Ag_5Au_{95} to pure Ag while the magnitude of region V decreases (Figure 3A). At peak V and beyond, the electron energy is sufficiently high to be considered as an extended X-ray absorption fine structure (EXAFS) oscillation where single scattering begins to prevail as it examines the region between 150-2,000 eV.

The position of the oscillations (positions of the resonance relative to the threshold) can be used to qualitatively infer the degree of Ag-Au lattice distortion in the fcc structure. Gold and silver are comparable in size Ag [16] but different in backscattering amplitude and phase, introducing are slight distortions in XANES oscillations in alloys compared to pure Ag. These multiple scattering events are larger in Au than Ag and therefore have different *k* dependence, *k* being the wavenumber of the photoelectron relating to the square root of the photon energy above the threshold [17]. These factors will influence the oscillations in the XANES spectrum.

The transition in the Ag_2S spectrum is due to a Ag $2p_{3/2}$ electron being excited to unoccupied bands above the Fermi level, whose bands possess both s and d character. The Ag_2S on the daguerreotype plate surface is a combination of procedural and environmental products. Due to the overriding signal of the Ag substrate [18], the Ag L_3-edge is not appropriate for comparison to the Ag_2S and AgCl standards, which bear no resemblance to the daguerreotype regions A1-3.

The XANES of all the daguerreotype samples areas, A1 (dark), A2 (mid-tone) and A3 (bright), look similar to that of pure Ag and $Ag_{95}Au_5$ while noticeably different from the alloys with dilute Ag in Au. While the A1-3 oscillations of region V have shifted to slightly higher energy, indicative of varying Ag-Au neighborhood in daguerreian alloy in comparison to the alloy standards, the magnitude of regions I, II, and V for A1-3 falls between Ag and $Ag_{95}Au_5$, indicating that the alloy present within the daguerreotype surface and near surface region has between 95 – 100% atomic percent Ag and 5 – 0% atomic percent Au. Based on the diffusion coefficient of 10^{-13} cm^2/s calculated for Au into Ag and Ag into Au on a historic daguerreotype plate [19], the observed alloy percentage of relatively low levels of Au may be partly due to the relatively slow inter-

diffusion for Ag and Au. However, as the degree of gilding is operator dependent, it is difficult to determine if the degree of alloying is due to the age of the plate or the independent recipe and methodology of the producer. Due to the dominant Ag signal in samples A1-3, the majority of information regarding the subtle variations in chemical structure on the daguerreian surface will come from Au, Hg, and S, which are discussed below.

3.2 Gold

The Au L_3-edge XANES of regions A1-3 and alloy standards are shown in Figure 4. Gold is the most electronegative metallic element having a Pauling scale value of 2.54, compared to Ag 1.93 [20] and, therefore, it is expected that Au will gain charge from Ag upon alloy formation. It is also expected that Au upon deposition on Ag will form Au-Ag alloys. Previous analysis of the Au L_3 edge whiteline of Au-Ag alloys establishes that the WL intensity increases upon dilution of Au in Ag. This result indicates that Au in fact gains s charge, $\Delta n_s > 0$ and loses 5d charge, $\Delta n_d < 0$ upon dilution in Ag but the overall charge flow, δ, though small, is from Ag to Au, in line with electronegativity considerations [21]. The Au L_3-edge jump appears at 11,919 eV (region I) and corresponds to the electronic transition from the $2p_{3/2}$ core level to the vacant $5d_{5/2}$ and $5d_{3/2}$ states just above the Fermi level. A gradual increase in the area under the curve at regions I from pure Au to the $Ag_{95}Au_5$ alloy is indicative of relatively more vacant $5d_{5/2,3/2}$ states (Figure 5). The resonances in regions II and III arises from the electron transitions to unoccupied densities of states above the Fermi level (multiple scattering). Peaks at (IV) and beyond are EXAFS arising from bound-to-continuum transitions modulated by single backscattering of neighboring atoms. The fact that the XANES and EXAFS look more Au-Ag alloy like than that of the pure Au indicates that Au-Ag alloy

is formed. A closer inspection of region V reveals that the Au in A1-3 is similar to those alloy standards with compositions between $Ag_{75}Au_{25}$ and $Ag_{95}Au_5$ [22].

From Figure 5, information can be gained by closely inspecting the edge jump. It should be noted that although Au has a full d-band, s-d hybridization and electron redistribution upon alloying with Ag will introduce unoccupied densities of state of 5d character at the Fermi level. From Figure 5A we see that as the relative concentration of Au compared to Ag is greatly reduced, the XANES data reveal more information regarding the degree of alloying in the daguerreotype plate. The whiteline region shows an increase in intensity hence an increase in the unoccupied density of d states. This observation indicates a d charge transfer from Au to Ag upon dilution. Now, examining the daguerreotype regions, A2 and A3 in Fig. 5B have the same magnitude and oscillation of peaks I and II with intensity differences arising in peaks II and IV. This is due to similar particle characteristics and composition in these two regions (A2 being a midtone and A3 being a bright region). Relative to pure Au, an increased area under the WL at peak I is indicative of proportionally less 5d charge (i.e. dilution). This is more prominent in region A1, suggesting that the greatest degree of alloying occurs in shadow regions and supports the notion that an Ag-Au alloy forms in the subsurface of the daguerreotype plate. Shadow regions contain few or no image particles and thus enable an increased amount of Au to diffuse into the subsurface, thereby allowing for the relative enrichment of Au in the Au-Ag alloy in this region of the daguerreian plate. This is the result of simultaneous diffusion of Au into the Ag substrate and Ag into the Au adlayer [19].

In comparison to the alloy standards, the normalized μ(E) spectra from daguerreotype areas A1-3 were subjected to linear combination fitting (LCF). Analyses were conducted

over an energy range of -20 eV below and +40 eV above the edge, thereby semi-quantitatively fitting the alloy standards to peaks I, II, and III. Region A1 revealed that alloy standards $Ag_{95}Au_5$ and $Ag_{75}Au_{25}$ were the primary contributors to the spectrum, having weight percent (at. %) values of 24.9 and 75.1 for $Ag_{75}Au_{25}$ and $Ag_{95}Au_5$, respectively. A similar result was observed in region A2, which contained $Ag_{75}Au_{25}$ and $Ag_{95}Au_5$ at. % values of 27.0 and 73.0, respectively. While the LCF curves (not shown) are a very good fit to the A1 and A2 spectra, it is expected that other Ag-Au alloys composition, which are comprised of at. % values between 25 and 5 for Au and 75 and 95 for Ag, are present. Therefore, given the spot size of the area analyzed and the diffusion mechanism, a good estimation of the average alloy composition present within the shadow and midtown regions is the average of these two standards: $Ag_{90}Au_{10}$.

While regions A1 and A2 only exhibit contributions from $Ag_{95}Au_5$ and $Ag_{75}Au_{25}$ (i.e., all other alloys had an at. % of 0), region A3 had contributions from $Ag_{50}Au_{50}$, $Ag_{75}Au_{25}$, and $Ag_{95}Au_5$, with at. % of 17.7 ($Ag_{50}Au_{50}$), 27.7 ($Ag_{75}Au_{25}$), and 54.6 ($Ag_{95}Au_5$). This LCF curve (not shown) is a very good fit to the A3 spectrum. Again, following the simultaneous diffusion mechanism of Ag into Au and Au into Ag, the proposed alloy for the highlight region is an average of the three contributing standards, consequently $Ag_{73}Au_{27}$. While these calculations are semi-quantitative at best, it does indicate a significant increase in Au content hence contributing to its lighter appearance. The amount of Au in the Ag-Au alloy increases from dark (A1) to highlight (A3) regions, emphasizing that alloying occurs on the image particles as well as with depth on the daguerreian plate, hence region A3 (highlight region) having the alloys with higher Au content.

It should be noted that when Au is introduced to the daguerreotype system, the gold-chloride-sodium thiosulfate solution is poured from above and covers the entire plate. From this, we assume an even amount of Au is present on all regions of the daguerreotype. Regions of high image particle density (bright regions) will have a relatively greater amount of Au on the surface of the plate due to diffusion limitations from the increased surface area of the image particles. Conversely, in dark regions where few/none image particles are observed, there is still an equal amount of Au but as a greater degree of diffusion is permitted to occur, there is relatively less Au on the surface and greater amount of subsurface alloying. Therefore the amount of total Au on the daguerreotype does not change from bright to dark regions, but the amount of Au in the Au-Ag alloy (degree of alloying) does.

3.3 Mercury

The Hg L_3-edge spectra are displayed in Figure 6. The absence of a whiteline indicates the deficiency of d vacancies above the Fermi level of Hg d character (s character is itinerant), suggesting the existence of metallic phase Hg. Peak positions of regions I-IV confirm the presence of an Hg-Ag amalgam particle [2, 12, 19], reported to possess 10.5 atomic percent Hg [19]. Peak III, IV, and the subsequent EXAFS oscillations also show characteristics consistent with the Hg-Ag interaction [12]. The EXAFS oscillation varies slightly from region to region and has multiple beatings indicating that Hg has both Hg and Ag neighbor. The periodicity of the oscillations suggests that the local environment varies somewhat from A1 to A3. The whiteline of A1-3 has no resemblance to HgO or $HgCl_2$ as peak I (12,288 eV) occurs as a shoulder opposed to a separate oscillation. Furthermore, the energy differences between peaks I and II in A1-3 first derivative spectra (not shown) are greater than that reported by Rajan et al. for α/β-HgS [23]. It is

unclear from these spectra if there is any variation in Hg-Ag alloying across the three examined regions. In all likelihood, a variety of Hg-Ag structures are present on the surface as suggest by Ravines et. al. [2].

3.4 Sulfur

The sulfur K-edge (Figure 7), which arises from an electron being excited from a 1s orbital to a 3p orbital, was recorded at 2,469.5 eV, indicative of transition-meal sulfides, such as Ag_2S [24]. Li et al [25] have conducted extensive analysis of the edge peak shift as a function of oxidation states, which spans 10-12 eV and includes sulfides (2-), native S (0), sulfite (4+), and sulfates (6+). The location of the K-edge from the daguerreian test plate is indicative of a metal sulfide interaction, which becomes increasingly complicated upon p-d hybridization between S antibonding and metal 3d states. This suggests that the S pπ* orbital is directly involved in the covalent Ag-S interaction [26]. This metal-sulfur bond is confirmed by the double feature of peak I that are characteristic of transition metal sulfur interaction [27]. What differs across A1-3 is the distinction of this peak I, which is greatest in A2 while A1 and A3 appear as a shoulder. The location of the electronic transition of peak III (2,482 eV) is due to sulfates in the form of Ag_2SO_4 [26, 28] or less likely an organic sulfonate species [29]; the amplitude of this peak decreases from A2, A1 to A3. Adsorption of SO_2 from ambient atmosphere on sliver surfaces has been previously reported [30]. A shift in peak position by approximately -0.2 eV for A2 and A3 suggests a different chemical environment in these regions. This may be the result of an Ag_2S-nanoparitcle interaction in these relatively brighter regions [31]. The broad nature of the peak at ~2,500 eV arises from the cumulative multiple scattering contributions of all sulfur species [32]. Work previously conducted by Outka et al. [32]

suggests that Ag is incapable of reducing S; any Ag_2S present is atmospheric in origin or a consequence of the gold-chloride-sodium thiosulfate solution used when gilding.

4 Conclusions

Synchrotron-based X-ray absorption spectroscopy proved to be a valuable technique to the study of daguerreotypes; no physical or chemical variation was observed on the surface after exposure to X-rays. This study provides information pertinent to the advancement of the chemical understanding of historic plates. Firstly, the Ag L_3-edge showed that the image particles on the surface form an alloy with a face centered cubic structure. The degree of Au diffusion into the Ag plate differed across the surface. Secondly, while Au L_3-edge examination revealed the shadow region (A1) to have the greatest degree of Ag-Au alloying, the highlight region (A3) possessed the greatest Au surface concentration and variation in alloys composition. The relative amount of Au in the Ag-Au alloy also varies between different tonal regions on the daguerreian surface. As estimated from the Au XANES analysis, an average alloy composition of $Ag_{90}Au_{10}$ was determined for the shadow and midtone regions while the highlight region suggested an average alloy composition of $Ag_{73}Au_{27}$. This variation in the Ag-Au alloy across bright to shadow regions should be considered before conservation treatments are applied as each region of the plate will react differently to the proposed method. Thirdly, examination of the Hg L_3-edge suggests that metallic Hg was amalgamated with the Ag image particles. Finally, the S K-edge revealed the presence of sulfates and sulfides on the surface, in the form of Ag_2S and Ag_2SO_4, respectively. Data may suggest the presence of Ag_2S-nanoparticle interactions in brighter regions as well as organic sulfonate species across all regions of the sample. Organic sulfur may be residue from the final wash step in the test plate's production. Production residue may serve as the primary

source of chemical deterioration on the daguerreian surface. This work highlights the capabilities of synchrotron-based absorption spectroscopy in the analysis of the daguerreotype surface.

5 Acknowledgements

This research was supported by the National Science and Engineering Research Council of Canada, the Canadian Foundation for Innovation, Canada Research Chairs (TKS) and the Ontario Ministry of Innovation. Further support for interdisciplinary research was provided by The Dean's Office at The University of Western Ontario, Faculty of Science. Synchrotron experiments were performed at the Canadian Light Source, which is supported by NSERC, NRC, CIHR and the University of Saskatchewan.

6 References

[1] Da Silva, E.; Robinson, M.; Evans, C.; Pejovic-Milic, A.; Heyd, D.F. *J. Anal. Atom. Spectrosc.* **2010,** 25, 654-661.

[2] Ravines, P.; Li, L.; McElroy, R. *J. Imaging Sci. Technol*. **2016,** 10, 30504-1 – 30504-10.

[3] Barger, S.M.; White, W.B. *The daguerreotype: nineteenth century technology and modern science;* Smithsonian Institution Press, Washington, 1991, a: pp. 120, b: pp. 162.

[4] Ravines, P; Wiegandt, R.; Wichern, C.M. *Surface Eng.* **2008,** 24, 138-146.

[5] Barger, S.M.; Krishnaswamy, S.V.; Messier, R. *J. Am. Conserv.* **1982,** 22, 13-24.

[6] Centeno, S.; Schulte, F.; Kennedy, N.; Schrott, A. *Appl. Phys. A.* 2011, 105, 55-63.

[7] Barger, S.M.; Messier, R.; White, W.B. *Photogr. Sci. Eng.* **1982,** 26, 285-291.

[8] Ravines, P. *Am. Lab.* **2010,** 42, 20-25.

[9] Anglos, D.; Melesanaki, K.; Zafiropulos, V.; Gresalfi, M.J.; Miller, J.C. *Appl. Spectrosc.* **2002,** 56, 423-432.

[10] Hogan, D.L.; Golovlev, V.V.; Gresalfi, Chaney, J.A.; Feigerie, C.S.; Miller, J.C.; Romer, G.; Messier, P. *Appl Spectrosc.* **1999,** 53, 1161-1168.

[11] S. D. Humphrey, American Hand Book of the Daguerreotype: Giving the Most Approved and Convenient Methods for Preparing the Chemicals, and the Combinations Used in the Art. Containing the Daguerreotype, Electrotype, and Various Other Processes Employed in Taking Heliographic Impression, 5th Eds.; S. D. Humphrey, New York, 1858.

[12] George, G.N.; Singh, S.P.; Hoover, J.; Pickering, I. *J. Chem. Res. Toxicol*. **2009,** 22, 1761-1764.

[13] Bzowski, A.; Sham, T.K.; Yiu, Y.M. *Anal. Review B.* **1994,** 49, 13776-13779.

[14] Ravel, B.; Newville, M. *J. Synchrotron Radiat.* **2005,** 12, 537-541.

[15] Ravel, B. Athena User's Guide. http://cars9.uchicago.edu/~ravel/software/exafs/. (accessed 10 September 2014).

[16] Hammond, C.R. *Handbook of Chemistry and Physics*; 81st Eds.; CRC press, New York, 2004; pp. 115.

[17] Newville, M. *Fundamentals of XAFS*; 2nd Eds.; University of Chicago, Chicago, 2004; pp. 7.

[18] Behrens, P.; Aβmann, S.; Bilow, U.; Linke, C.; Jansen, M. *Z. Anorg Allg Chem*. **1999,** 625,111–116.

[19] Marquis, E.A.; Chen, Y.; Kohanek, J.; Dong, Y.; Centeno, S.A. *Corros Sci,* **2015,** 94, 438-444.

[20] Pauling, L. *The Nature of the Chemical Bond*, 3rd Eds.; Cornell University Press, Ithaca, 1960; pp. 88.

[21] Sham, T.K.; Ward, M.J.; Murphy, M.W.; Liu, L.J.; Han, W.Q. *J. Phys.: Conf. Ser.* **2013,** 425, 092006.

[22] Tyson, C.C; Bzowski, A.; Kristof, P.; Kuhn, M.; Sammynaiken, R.; Sham, T.K. *Phy. Rev. B,* **1992,** 45, 8924– 8928.

[23] Rajan, M.; Darrow, J.; Hua, M.; Barnett, B.; Mendoza, M.; Greenfield, B.K.; Andrews, J.C. *Environ. Sci. Technol.* **2008,** 43, 7397–7402.

[24] Shimizu, K.; Kobayashi, N.; Satsuma, A.; Kojima, T.; Satokawa, S. *J. Phys. Chem. B*. **2006,** 110, 22570-22576.

[25] Li, D.; Bancroft, M.; Kasrai, M.; Fleet, M.E.; Feng, X.; Tan, K. *Can. Mineral*. **1995,** 33, 949-960.

[26] Fleet, M.E. *Can. Min.* **2005,** 43, 1811-1838.

[27] Hullebusch, E.; Rossano, S.; Farges, F.; Lenz, M.; Labanowski, J.; Lagarde, P.; Flank, A-M.; Lens, P. *J. Phys: Conf. Ser*. **2009,** 190, 012184.

[28] Fors, Y.; Grudd, H.; Rindby, A.; Jalilehvand, F.; Sandström, M.; Cato, I.; Bommalm, L. *Sci. Rep.* **2014,** 4, 4222-1 – 4222-6.

[29] Manceau, A.; Nagy, K.L. *Geochim. Cosmochim. Acta.* **2012,** 99, 206-223.

[30] Outka, A.D.; Madix, R.J.; Fisher, G.B.; DiMaggio, C. *J. Phys. Chem*. **1986,** 179, 1-24.

[31] Wang, P.; Menzies, N.W.; Lombi, E.; Sekine, R.; Blamey, F.P.C.; Hernandez-Soriano, M.C.; Cheng, M.; Kappen, P.; Peijnenburg, W.J.G.M.; Tang, C.; Kopittke, P.M. *Nanotoxology*. **2015,** 9, 1041-1049.

[32] Veronesi, G.; Koudouna, E.; Cotte, M.; Marin, F.L.; Quantock, A.J. *Anal. Bioanal. Chem.* **2013,** 405, 6613– 6620.

6 Tables

Table 1 List of beamlines used for each element of interest.

Element	Beamline	Edge(s)
Ag	SXRMB (BM, 1.7 – 10 keV) (daguerreotype plate, Ag-Au alloy standards, AgCl, and Ag_2S standards)	$L_{3,2}$-edge
Au	VESPERS (BM, 6 – 30 keV) (daguerreotype plate) HXMA (Wiggler, 5 – 40 keV) (Ag-Au alloy standards)	$L_{3,2}$-edge
Hg	VESPERS (daguerreotype plate)	L_3-edge
S	SXRMB (daguerreotype plate)	K-edge

Table 2 Series of silver-gold alloy standards [12].

Name of Standard	Atomic Percentage of Silver	Atomic Percentage of Gold
Ag	100%	0%
$Ag_{95}Au_5$	95%	5%
$Ag_{75}Au_{25}$	75%	25%
$Ag_{50}Au_{50}$	50%	50%
Ag_5Au_{95}	5%	95%
Au	0%	100%

7 Figure Captions

Figure 1 Areas of interest, with accompanied labeling, examined from the daguerreotype test plate. Image taken with a single-lens reflex camera. (A1: dark region; A2: mid-tone region; A3: bright region)

Figure 2 Comparison of the Ag L_3-edge XANES of daguerreian test plate (A1, A2, A3) alloy standards ($Ag_{95}Au_5$, Ag_5Au_{95}, $Ag_{50}Au_{50}$, $Ag_{75}Au_{25}$), and Ag_2S

Figure 3 Comparison of (A) the Ag L_3-edge alloy standards and (B) of daguerreotype regions A1, A2, A3 against $Ag_{95}Au_5$ and $Ag_{75}Au_{25}$ standards

Figure 4 Au L_3 XANES of daguerreian plate (A1, A2, A3) and alloy standards ($Ag_{95}Au_5$, Ag_5Au_{95}, $Ag_{50}Au_{50}$, $Ag_{75}Au_{25}$, Au). The dotted lines track the position of the resonances in pure Au and the solid line track the position of the oscillation in region V of the A1-3 XANES

Figure 5 Au L_3-edge of (A) Au alloys and (B) daguerreotype regions A1-3 with Au, $Ag_{75}Au_{25}$, and Ag_5Au_{95}. Arrows indicate the relative increase of the area under the curve at relevant frequencies

Figure 6 Hg L_3-edge of daguerreotype plate (A1, A2, A3) in comparison to elemental Hg standard

Figure 7 Sulfur K-edge of daguerreotype plates (A1, A2, A3) with Ag_2S standard

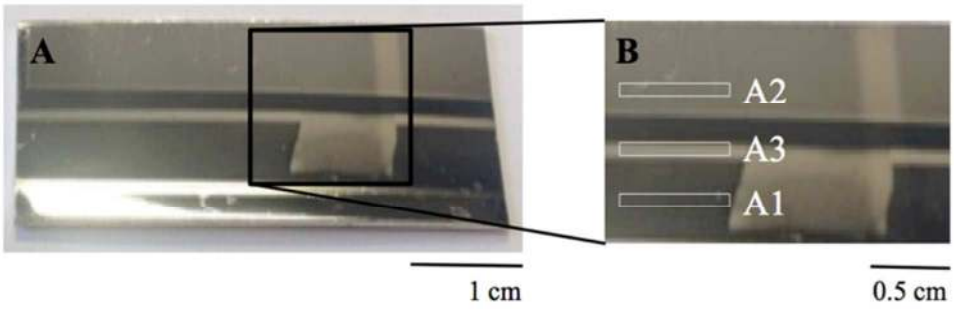

Figure 1 Areas of interest, with accompanied labeling, examined from the daguerreotype test plate. Image taken with a single-lens reflex camera. (A1: dark region; A2: mid-tone region; A3: bright region)

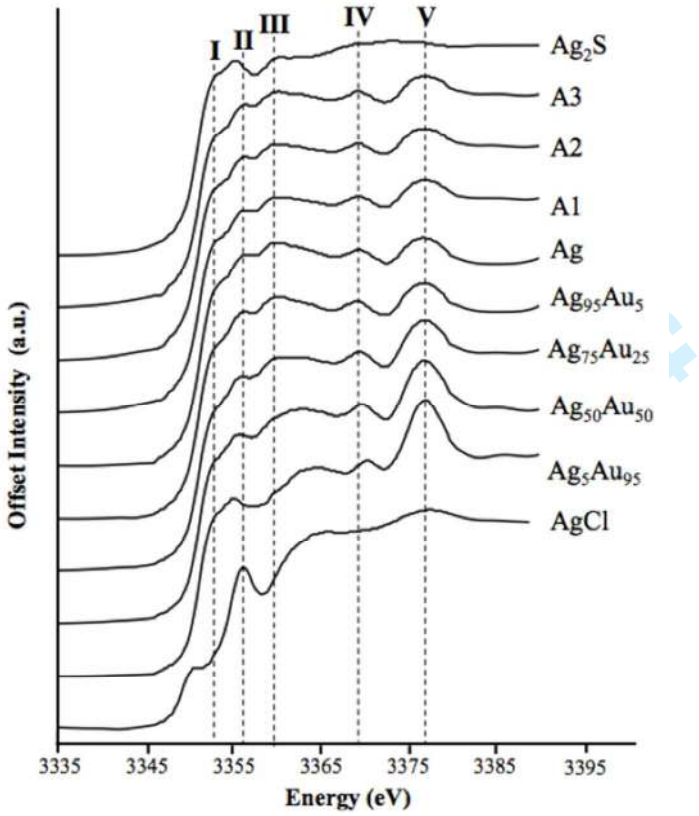

Figure 2 Comparison of the Ag L_3-edge XANES of daguerreian test plate (A1, A2, A3) alloy standards ($Ag_{95}Au_5$, Ag_5Au_{95}, $Ag_{50}Au_{50}$, $Ag_{75}Au_{25}$), and Ag_2S

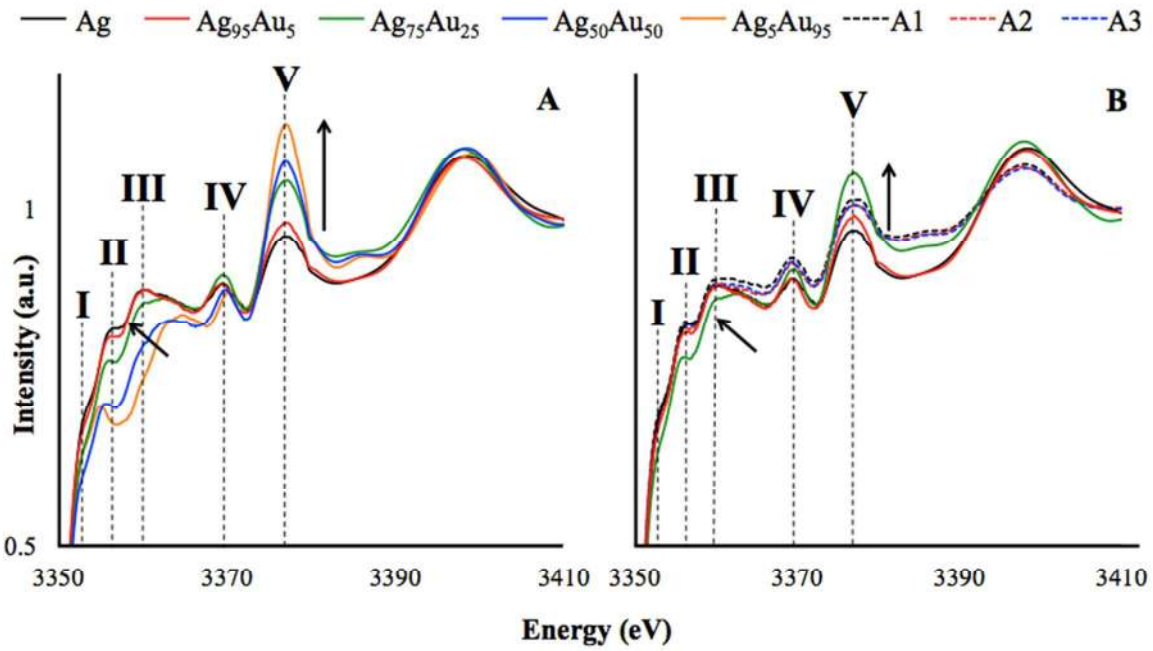

Figure 3 Comparison of (A) the Ag L_3-edge alloy standards and (B) of daguerreotype regions A1, A2, A3 against $Ag_{95}Au_5$ and $Ag_{75}Au_{25}$ standards

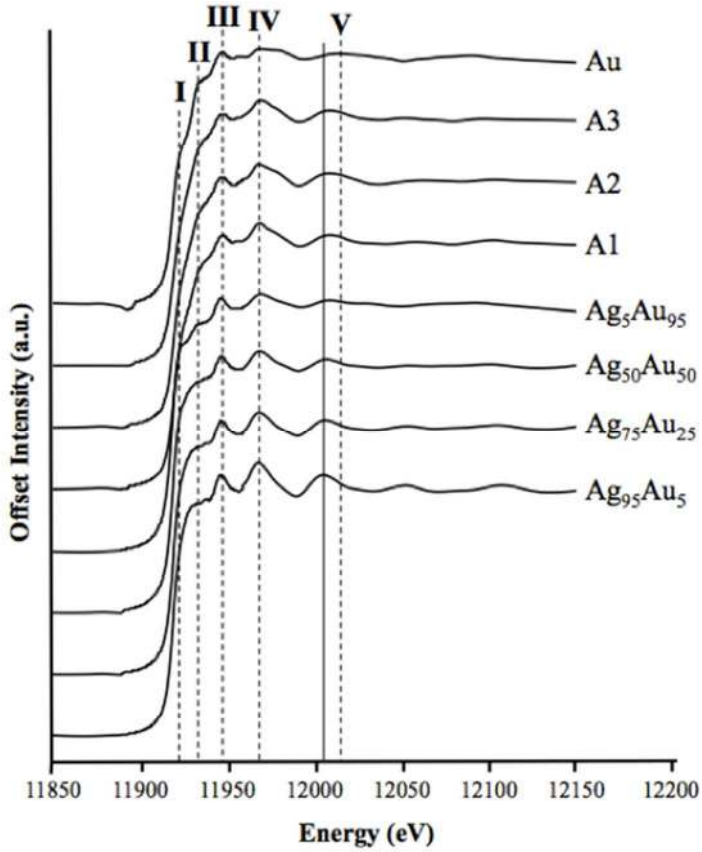

Figure 4 Au L_3 XANES of daguerreian plate (A1, A2, A3) and alloy standards ($Ag_{95}Au_5$, Ag_5Au_{95}, $Ag_{50}Au_{50}$, $Ag_{75}Au_{25}$, Au). The dotted lines track the position of the resonances in pure Au and the solid line track the position of the oscillation in region V of the A1-3 XANES

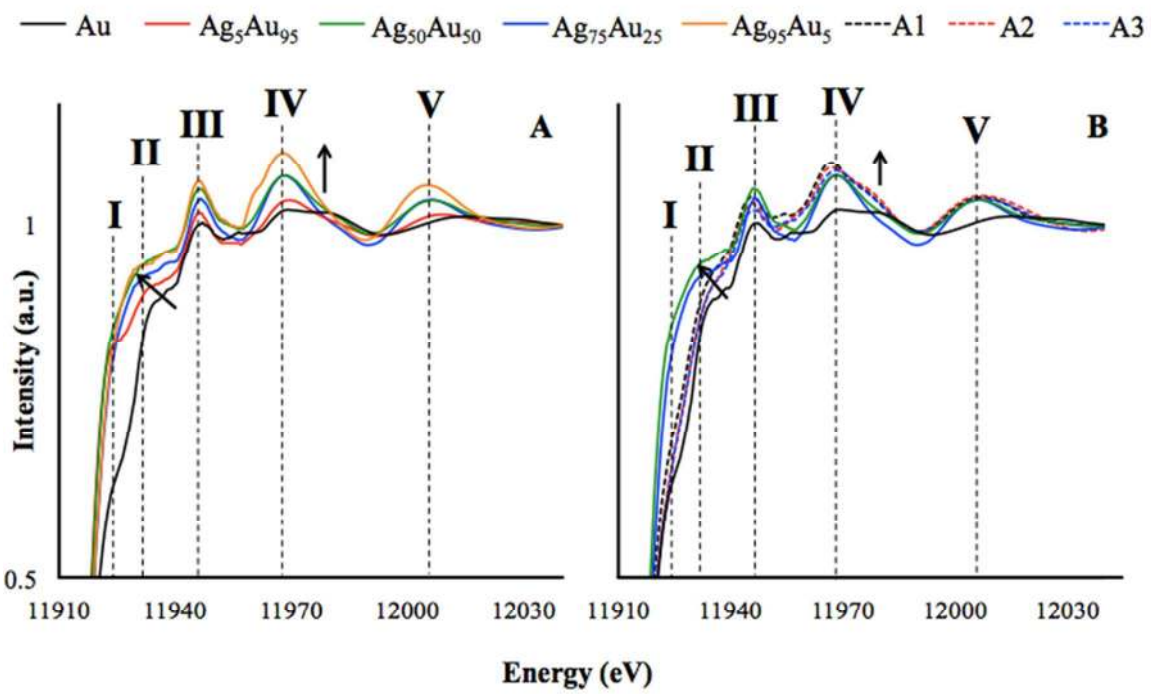

Figure 5 Au L_3-edge of (A) Au alloys and (B) daguerreotype regions A1-3 with Au, $Ag_{75}Au_{25}$, and Ag_5Au_{95}. Arrows indicate the relative increase of the area under the curve at relevant frequencies

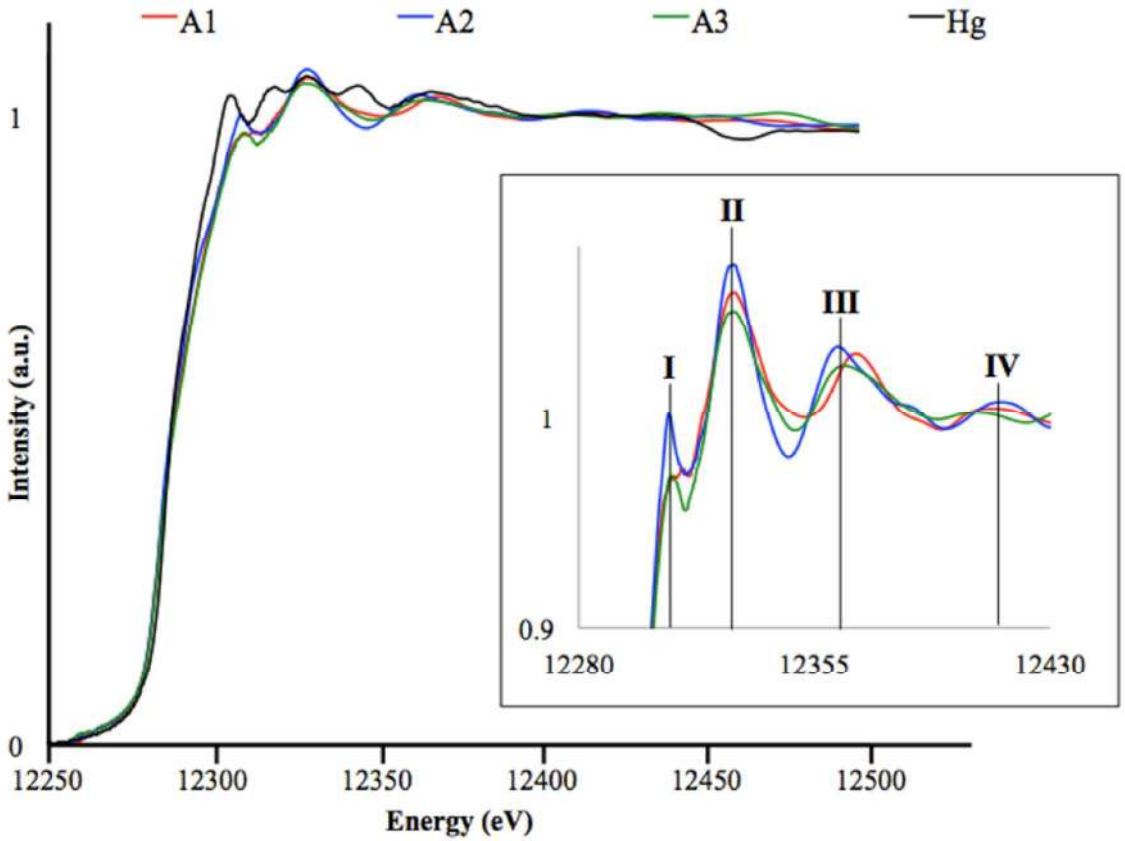

Figure 6 Hg L_3-edge of daguerreotype plate (A1, A2, A3) in comparison to elemental Hg standard

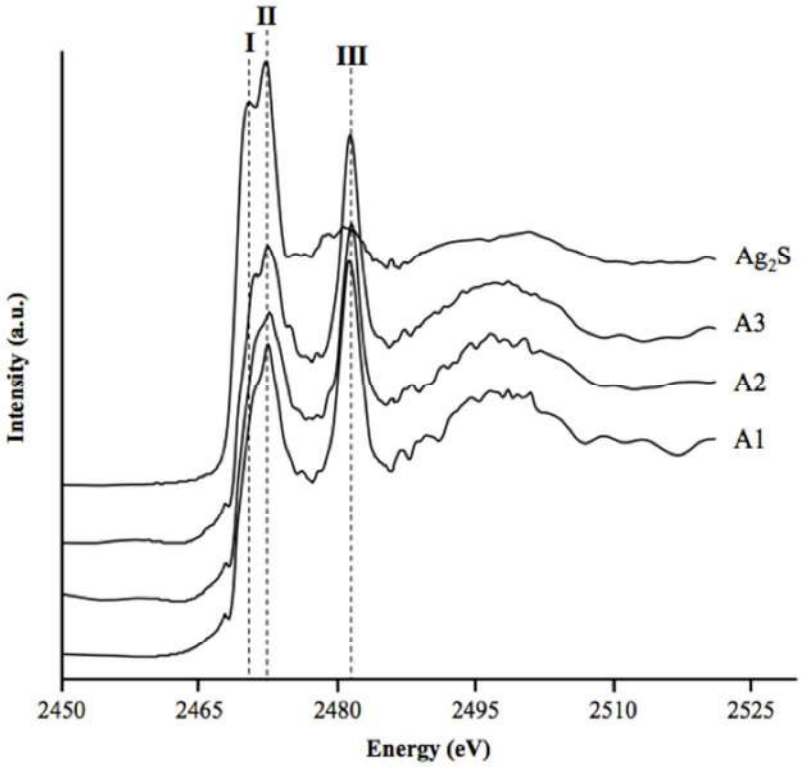

Figure 7 Sulfur K-edge of daguerreotype plates (A1, A2, A3) with Ag_2S standard